Carbon 137 (2018) 502–510

Contents lists available at ScienceDirect

Carbon

journal homepage: www.elsevier.com/locate/carbon

In-situ mechanics of 3D graphene foam based ultra-stiff and flexible metallic metamaterial

Pranjal Nautiyal [a], Mubarak Mujawar [b], Benjamin Boesl [a], Arvind Agarwal [a, *]

[a] Nanomechanics and Nanotribology Laboratory, Department of Mechanical and Materials Engineering, Florida International University, 10555 West Flagler Street, Miami, FL 33174, USA
[b] Advanced Materials Engineering Research Institute, Florida International University, 10555 West Flagler Street, Miami, FL 33174, USA

ARTICLE INFO

Article history:
Received 7 April 2018
Received in revised form
19 May 2018
Accepted 28 May 2018
Available online 29 May 2018

ABSTRACT

A 3D macroporous graphene foam based ultra-lightweight, stiff and fatigue-resistant mechanical metamaterial is developed in this study. In-situ indentation of the 3D graphene framework reveals an extraordinary spring constant of ~15 N/m and an upward of 70% recoverable deformation. The brilliant stiffness and superelasticity of graphene foam is exploited to fabricate Aluminum-based Graphene/Metal Metamaterial by electron beam evaporation. In-situ cyclic indentation inside SEM up to 50 cycles revealed long-distance stress-transfer due to the interconnected network of branches, having spring-like mechanical energy storage ability. The structure is highly fatigue-resistant, with more than 98% of displacement recovery at the end of each loading/unloading cycle. In-situ tensile investigation reveals shearing-type failure with dual-strengthening mechanisms, where stress transfer from Aluminum layer to graphene scaffold enhances the overall load bearing ability and the Aluminum deposit on graphene foam provides a structural backbone that restricts brittle failure. A modified scaling law is proposed for modeling the mechanical strength of cellular metamaterials that takes into consideration the hollow anatomy of graphene frameworks, thereby bridging the current gap in theoretical and experimental foam mechanics. The 3D metamaterial developed in this study can be a game-changing candidate for developing flyweight metallic structures with unprecedented elasticity, stiffness and fatigue-resistance.

1. Introduction

In recent years, controlled and rational design of material architectures has taken a center stage in materials science as a strategy to achieve desired functionalities in metamaterials [1–5]. These metamaterials comprise of repeating unit cells and their properties are strongly correlated to their structure rather than the composition. Mechanical metamaterials have gained traction for developing lightweight, stable and strong structures by carefully controlling the architecture [6,7]. From structural application standpoint, low density cellular or porous architectures are highly preferable. 'Free-standing' mechanical metamaterials are able to effectively translate excellent material properties at nanoscale to achieve desirable mechanical attributes at macroscale [8,9]. Combining the metamaterial design approach with excellent 'intrinsic' material properties can be a highly effective strategy for engineering structural materials with brilliant mechanical properties. Nano-structured materials, such as nanocrystals, nanofibers, nanoparticles, nanotubes and nanosheets display remarkable mechanical stiffness and strength and hence, have attracted attention as filler materials for lightweight structural metals to augment their mechanical properties [10–12]. However, this approach does not provide desired microstructure control and introduces structural defects, resulting in unwarranted variability in properties and performance. To overcome this challenge, carefully designed metamaterials made from the desired nano-structured materials can be employed as fillers for obtaining homogeneous material microstructures. Graphene is a well-known two-dimensional nanomaterial, with an excellent in-plane elastic modulus as high as 1 TPa and a tensile strength of 130 GPa [13]. These mechanical properties of graphene make it a promising material candidate for developing cellular mechanical metamaterials [14].

There has been tremendous interest in 3D frameworks of graphene in recent years. Some of the examples of popular graphene architectures from application standpoint are hydrogel, aerogel, cork, macroporous foam, and nanoporous sponge [15]. These

* Corresponding author.
E-mail address: agarwala@fiu.edu (A. Agarwal).

https://doi.org/10.1016/j.carbon.2018.05.063
0008-6223/

graphene assemblies are capable of withstanding > 50,000 times their weight and are characterized by an outstanding recovery from 80% compressed state [16]. Due to their superior specific tensile strength and Young's modulus, 3D graphene monoliths are capable of energy dissipation with reported energy loss coefficients as high as 87%. Freestanding 3D graphene foam with macroporous architecture has been demonstrated to be an excellent candidate for applications in structural materials [17], supercapacitors [18], strain sensors [19], electromagnetic interference shielding [20], tissue engineering [21], damping [22], de-icing [23] and thermal interface material [24]. The interconnected network of hollow branches makes the mechanics of graphene foam unique. During compressive loading, the graphene foam undergoes a three-stage deformation [25]. At very low strains ($\varepsilon < 0.1$), elastic bending of graphitic ligaments takes place resulting in a linear stress-strain regime. At intermediate strains, the plastic collapse of these ligaments results in a plateau in the stress-strain behavior, followed by a steep rise in stress as a result of compaction of the fragmented ligaments. Bending, self-folding, and rotation of graphene flakes are proposed as the micromechanisms during plastic deformation [26]. These micromechanisms can be altered by controlling the stiffness of foam branches, suggesting a tunable Poisson's ratio of 3D graphene foam. Localized indentation loading of the foam causes the bending of branches, followed by depression of the foam wall at higher loads [27]. During indentation, the area of interaction between the indenter tip and the foam wall determines the nature of deformation. Nieto and co-workers reported depression of foam wall upon indentation by conospherical probe, which manifests as an increase in slope of the load-displacement curve [27]. This regime was absent when a flat punch was used to apply the loads due to greater area and lower stress. Tensile deformation of graphene foam causes the branches to align along the loading direction. Due to this alignment, the superior in-plane stiffness and strength of graphene is utilized to provide enhanced load bearing ability [27]. Due to its hierarchical structure, graphene foam exhibits multi-scale energy dissipation/dispersion mechanisms, such as formation of dynamic ripples, interlayer spring-like van der Waals interactions, kink band formation and hollow wall vibration effect [28].

These observations suggest that graphene foam architecture is structurally robust and highly flexible. We envisage the application of this unique 3D scaffold for engineering flexible graphene-metal heterostructures. Lightweight metallic microlattices (with achievable densities less than 10 mg/cm^3) are characterized by efficient load transfer, recoverable deformation and energy absorption capabilities [29,30]. It is reported that the mechanical properties of metallic microlattices is greatly influenced by the properties of the parent material [30]. Hence, we propose to employ 3D graphene foam as a base structure on which Al is deposited, to augment the stiffness and strength of the material. Firstly, this porous heterostructure will display excellent stiffness and strength due to the brilliant intrinsic mechanical properties of 2D graphene, and secondly, the 3D architecture comprising of open cells and hollow branches will provide remarkable flexibility and stress distribution ability. Considering ultra-low density of graphene foam (<5 mg/cm^3), such flexible metal-graphene heterostructures can be promising metamaterial for engineering lightweight, robust and flexible metal matrix composites. The promise of hetero-structured metamaterials was recently demonstrated by Zhang and co-workers by designing a graphene/ceramic metamaterial (GCM) with honeycomb architecture [14]. This metamaterial was found to exhibit flyweight density, high fatigue resistance and reversible compressibility, overcoming the key shortcomings of conventional ceramics. Inspired by these recent findings and extraordinary mechanical attributes of graphene foam, we have developed an ultra-lightweight graphene/metal metamaterial (GMM) based on macroporous 3D graphene foam and Aluminum in this study.

2. Experimental

2.1. Fabrication of 3D metamaterial

The free-standing macroporous 3D graphene foam used in this study was obtained from Graphene Supermarket (Calverton, NY, USA). 1 μm thick layer of Al was deposited on graphene foam using CHA SAP 600 e-Beam Evaporation system (California, USA). The graphene foam was mounted on a quartz substrate and placed in the evaporator. Prior to deposition, the system was evacuated to a base pressure of 5×10^{-7} Torr. 99.99% pure Al target was bombarded with an electron beam (10 kV, 330 mA) to achieve a deposition rate of 1 nm/s at an operating pressure of 1×10^{-6} Torr. The thickness of the Al deposition was monitored using a quartz crystal monitor.

2.2. In-situ mechanical investigations

For nanoindentation characterizations, the free-standing 3D graphene foam (GrF) and Al/GrF metamaterial were mounted on the stage of SEM Picoindenter (Hysitron PI 87, Minnesota, USA). The stage was installed inside a dual beam JEOL JIB-4500 focused ion beam/SEM system. A diamond Berkovich tip of 100 nm diameter was used to apply localized loads and real-time deformation videos were captured by the SEM. Quasi-static nanoindentation tests were performed by programming the peak load of 2000 μN and the loading/unloading rate of 25 μN/s. For fatigue tests, a total of 50 cycles were performed and the corresponding load-displacement-time profiles were captured. In order to visualize the deformation in the materials, microstructural strain analysis of the real-time SEM videos was performed using VIC-2D digital image correlation (DIC) software (Correlated Solutions, Irmo, USA). The resultant DIC strain maps provide information about the dispersion/transfer of deformation in the 3D architecture.

3. Results and discussion

3.1. In-situ mechanics of 3D graphene framework

The 3D graphene foam used in this study was obtained by chemical vapor deposition of graphene on a Nickel foam. This was followed by etching away of Ni, resulting in a free-standing cellular graphene structure with a node-branch anatomy (Fig. 1a). The nodes and branches of graphene foam are hollow due to etching away of Ni (shown in the inset to Fig. 1a). The mechanical deformation of graphene foam was studied by *in situ* nanoindentation in a scanning electron microscope. The node of the graphene foam was subjected to compressive force by a Berkovich indenter tip (Fig. 1b). Supplementary Video V1 shows the indentation behavior of graphene foam. A peak load of 2000 μN was applied so as to induce large enough deformation to capture the response of the 3D structure (interconnected nodes and branches), and not just perform a local indentation. Unlike the conventional indentation of materials, there is no prominent localized failure or penetration of the tip into the material. Rather, the applied load is transmitted to the adjacent branches, which can be seen from the SEM snapshot of the foam at the peak applied load of 2000 μN (Fig. 1b). This effective dispersion of stress over a large area prevents localized failure and enhances graphene foam's damage tolerance. This is evidenced by the post indentation SEM snapshot (Fig. 1b), showing that the graphene foam recovers to its original configuration after unloading. The corresponding load-displacement curve for the

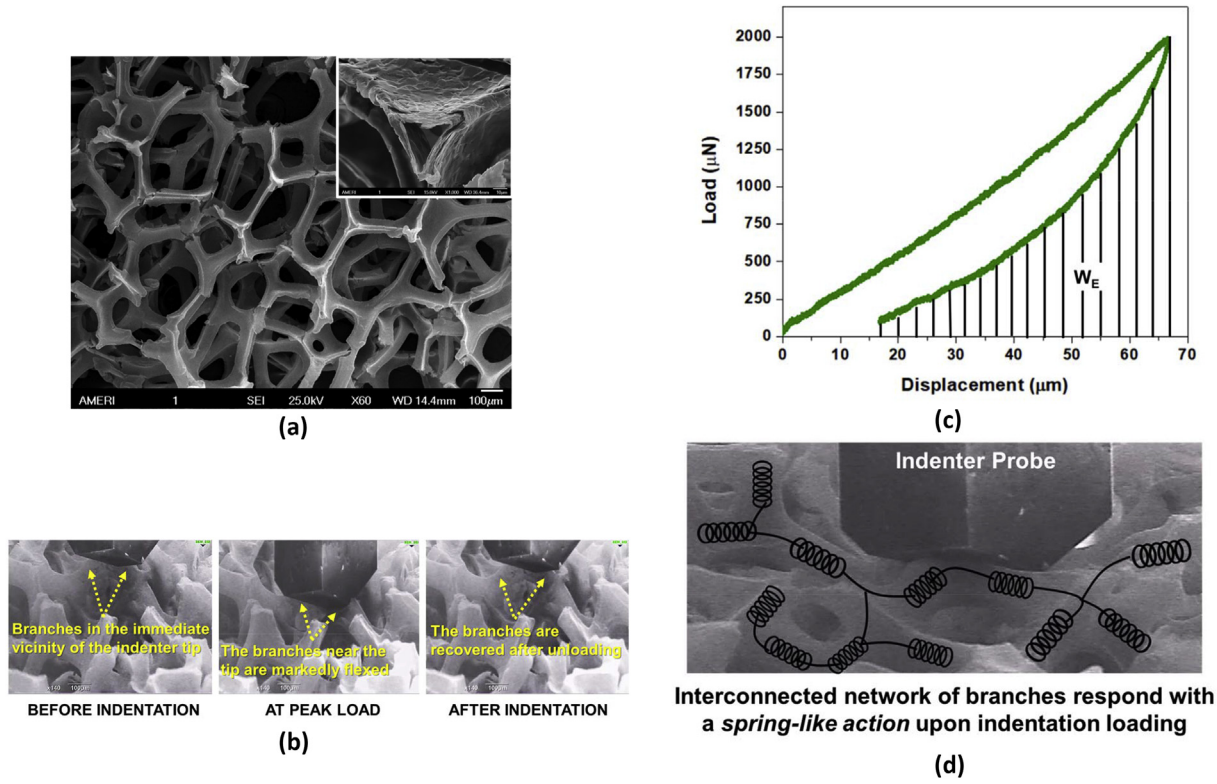

Fig. 1. (**a**) SEM micrograph of 3D graphene foam with open cell structure (inset shows the hollow branches of graphene foam), (**b**) real-time SEM snapshots during *in-situ* nanoindentation of graphene foam before indentation, at peak load of 2000 μN and after unloading (the branches in the immediate vicinity of the tip are marked to show significant flexing and subsequent recovery during the loading/unloading cycle), (**c**) indentation load-displacement curve with elastic work of indentation shaded (area under the unloading curve), and (**d**) schematic illustration of spring-like action of graphene foam branches, imparting excellent stiffness and elasticity to the framework. (A colour version of this figure can be viewed online.)

indentation is shown in Fig. 1c. While the maximum displacement (h_{max}) at peak applied load is 66 μm, the final residual displacement (h_f) of the foam after unloading is 17 μm. This excellent displacement recovery (>70%) indicates the suitability of graphene foam as a superelastic metamaterial. Therefore, the branches of graphene foam can be modeled as springs-damper assembly (schematically shown in Fig. 1d), where the spring-like action promotes the recovery towards the original state after the applied force is removed (elastic component) and the damper causes the dissipation or loss of energy during the loading-unloading cycle (loss component). During indentation, the elastic work (W_E) can be computed by determining the area under the unloading (F-h) curve: [31].

$$W_E = \left| \int_{h_{max}}^{h_f} Fdh \right| \quad (1)$$

The elastic work of indentation (W_E) was computed to be 37.2 nJ. Assuming spring-like behavior of graphene foam branches, the elastic work can be considered to be stored as the potential energy. During indentation, multiple branches are stretched/deformed (as shown in Video V1). Assuming the net or effective spring constant of the branches experiencing stress transfer to be K_{eff}, the overall spring potential energy can be modeled as:

$$W_E = \frac{1}{2} K_{eff} h_E^2 \quad (2)$$

From the load-displacement curve, the net 'elastic displacement' (h_E) during indentation of graphene foam is h_{max} - $h_f \approx 50$ μm. Substituting h_E and W_E to Eq. (2), K_{eff} is obtained to be ~15 N/m. The spring constant is a measure of stiffness of the material; in other words, a material with superior spring constant can bear greater loads without collapsing. The reported spring constant for graphene layers is in the range of 1–5 N/m [32]. It is quite striking that 3D graphene foam exhibits at least 3 times the spring constant of 2D graphene sheets, making it an extremely promising mechanical metamaterial to impart superior strength and stiffness for structural applications.

Supplementary video related to this article can be found at https://doi.org/10.1016/j.carbon.2018.05.063.

The graphene foam was also subjected to cyclic loading/unloading to evaluate its nano-scale fatigue performance. The indenter tip was used to apply a total of 50 cycles on the foam and the deformation behavior was observed in real time under SEM (Supplementary Video V2). The peak applied load during the nano-fatigue tests was around ~1700 μN (Fig. 2a). The corresponding displacements were also recorded. Strikingly, it was observed that the deformation was predominantly elastic. About 98–99% of displacement was recovered after every loading-unloading cycle, with only ~1–2% enhancement of residual depth. This minimal plastic deformation could be due to rotation, bending and folding of graphene flakes constituting the 3D foam walls [26,27]. These deformation mechanisms lead to some residual deformation (indentation displacement) at the end of each cycle, which manifests as a moderate increase in displacement over time (as seen in Fig. 2a). Overall, the results indicate excellent fatigue resistance of graphene foam. The supplementary video V2 shows that the deformation is transmitted along the interconnected pathways offered by the node-branch architecture of 3D foam. To assess the

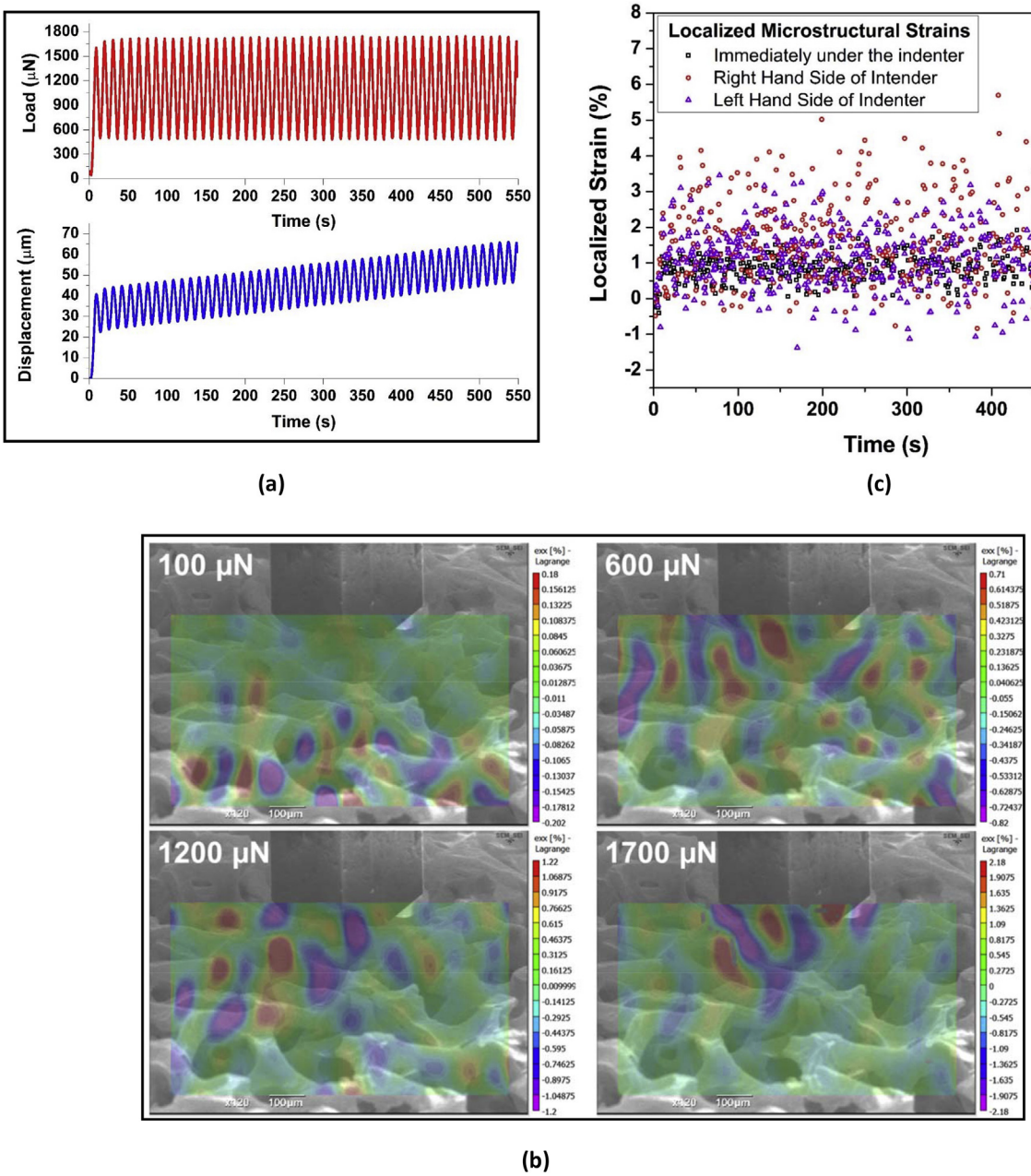

Fig. 2. **(a)** Cyclic loading-unloading profile and the corresponding displacement response during nanoindentation fatigue testing, **(b)** comparative strain maps obtained by digital image correlation (DIC) analysis of first fatigue loading cycle at different instants (the corresponding applied loads are labelled in the maps), and **(c)** evolution of local strain values under the indenter tip (black squares), 300 μm away from the tip (red circles) and 500 μm away from the tip (purple triangles) during the course of 50 fatigue cycles. (A colour version of this figure can be viewed online.)

overall contribution of graphene foam microstructure towards load bearing, the real-time SEM videos of the cyclic tests were used for digital image correlation (DIC) analysis. DIC investigation provided the information about strains developed in different regions of graphene foam microstructure, by comparing the real-time snapshots (during deformation) with respect to the unloaded, reference SEM image. Fig. 2b shows the relative-strain maps for graphene foam subjected to cyclic testing at different points of the first loading cycle. These maps provide information about strain evolution in the microstructure over time, as a function of applied indentation load. Different colored contours represent the variation in strains experienced by different areas of graphene foam. The indices on the right hand side of the maps quantify the strains in different color coded contours. These maps show the strains in x-direction, that is, perpendicular to the axis of indentation. It is to be noted that the real-time SEM deformation video of the foam was captured in a tilted orientation. Therefore, the strain contours obtained by DIC provide an estimation of 'relative-strains' in the microstructure, which is useful to develop insight into the deformation of the 3D architecture as a function of applied loads. However, these values cannot be construed as absolute values of strains, which is why we do not use these for any local stress computations. The evolution of positive and negative strain contours indicates multi-directional stress transfer in graphene foam. It is interesting to note that the z-direction, or axial displacement induced by the indenter at the point of contact is transmitted along

the non-axial directions throughout the sample, evident from the planar strains (ε_x) developed in the foam during loading. This is possible because of the interconnected network of graphene branches (Fig. 1a). From the strain maps, it can be seen that as the applied load increases, the magnitude of microstructural strain increases (Fig. 2b). At 100 mN, the peak positive and negative strains were found to be 0.18 and -0.202%, respectively. However, at ~1700 mN, the peak localized planar strains were as high as 2.18%. To track the microstructure strain evolution during the entire fatigue test, the localized strains at three different locations in the foam are plotted in Fig. 2c. These three points were chosen such that one of them was right under the indenter tip, the second point was 300 μm away from the indenter (towards the left) and the third point was about 500 μm away from the indenter tip (towards the right). All the three points were in the same horizontal line as the indenter tip for relative comparison, as plotted in Fig. 2c. The strain plot confirms the excellent long-distance stress transfer in graphene foam: while the indenter probe directly interacts with the foam in a very localized zone (100 nm probe diameter), the deformation is transmitted along the length scales which are 3 orders of magnitude larger (several hundreds of μm) than the contact zone. This unique ability of rapid momentum transfer along long distances provides graphene foam its excellent fatigue resistance.

It is very remarkable that in both quasi-static indentation as well as fatigue testing, the applied loads are as high as 2000 μN, yet there was no signature of crack propagation or delamination of graphene flakes. In conventional bulk materials, the fracture strength is expressed as:

$$\sigma^f = \frac{K_C}{\sqrt{\pi a}} \tag{3}$$

where K_C is the fracture strength and a is the initial flaw size in the material. The strength is inversely proportional to the size of structural flaws or defects in the material. However, in nanostructured materials, the probability of finding the defects or flaws is significantly reduced [31], and the failure initiation in these materials is typically explained by Weibull statistics. Weibull analysis predicts the fracture strength to be inversely related to the material volume (V):

$$\sigma^f \propto \left(\frac{1}{V}\right)^{1/m} \tag{4}$$

where m is the Weibull modulus and the higher value of m is desirable as it indicates that the physical flaws in the material are not clustered inconsistently. For the hollow graphene foam wall, $V \sim A \times t$, where A is the surface area and t is the wall thickness. The graphene foam walls comprise of a few layers of graphene and are typically <10 nm in thickness. This translates into excellent strength and load bearing ability of 3D graphene foam. As the thickness of the wall would decrease, the strength would go up until it reaches a critical thickness (t_{cr}) at which the material's strength would be bound by a theoretical upper limit given by: [33].

$$\sigma^f_{limit} = \frac{E}{2\pi} \tag{5}$$

where E is the in-plane elastic modulus of the material and this limit strength characterizes the dimension-independent atomic bond strength. In graphene foam, the theoretical peak stress experienced by the foam branch walls is computed to be remarkably high, around 150 GPa (based on Eq. (5)). This explains the remarkable ability of graphene foam structure to bear loads without cracking or collapsing. The findings in this section clearly demonstrate excellent mechanical attributes of graphene foam, making it a suitable candidate for developing novel lightweight metamaterials.

Supplementary video related to this article can be found at https://doi.org/10.1016/j.carbon.2018.05.063.

3.2. 3D graphene/metal metamaterial

Excellent ability of graphene foam to sustain stresses without failing was exploited to develop lightweight and ultra-flexible graphene/metal metamaterial. Aluminum metal was deposited on graphene foam by electron beam evaporation technique to obtain a 'free-standing' and structurally stable metamaterial (schematically shown in Fig. 3a). A 1 μm thick layer of Al metal was deposited on the foam branches to obtain 3D Aluminum-Graphene foam architecture (henceforth referred to as Al/GrF). Electron beam evaporation technique is capable of achieving deposition rates anywhere from 1 nm/min up to a few μm/min, and therefore, is a competent technique for scaling up nano-structured metamaterials. For instance, the 3D foam wall thickness was scaled up by 2 orders of magnitude in this study (from initial ~ 10 nm−1000 nm), which is crucial for practical applications. The mechanics of Al/GrF was investigated by *in-situ* nanoindentation inside the SEM chamber. The real time video of the test is provided as Supplementary Video V3. The foam was subjected to a maximum load of 2000 μN (Fig. 3b). The overall displacement was greatly restricted in Al-GrF ($h_{max} < 23$ μm) as compared to pristine graphene foam ($h_{max} \sim 66$ μm). Similar to graphene foam, Al/GrF is also observed to be flexible and there were no signs of local failure (Video V3). In addition, Al layer provides a structural backbone to the bare and slender graphene foam walls. However, only 10 μm (or 45%) of the displacement was recovered when the applied load was removed, as against pristine graphene foam which was characterized by >75% recoverable displacement during quasi-static indentation. Since the indenter probe contacts with the Al layer first, some degree of material removal (or plastic deformation) is anticipated, unlike ultra-thin graphene foam wall which resists failure (Weibull statistical theory). It is well known that local stresses can induce de-bonding of the deposit from the substrate surface [34]. Therefore, there is the possibility of energy loss due to relative sliding at the interface of foam wall and Al layer, resulting in low recoverable elastic displacement ($h_E = 10$ μm). As a result, the elastic work of indentation, W_E for Al/GrF was computed to be 5.67 nJ (based on Eq. (1)), which is much lower than the elastic work obtained for pristine graphene foam (37.19 nJ). Substituting these values of W_E and h_E to Eq. (2), the effective spring constant (K_{eff}) of Al/GrF heterostructure was computed to be ~1.13 N/m. K_{eff} for Al/GrF heterostructure is lower than pristine graphene foam (15 N/m); nevertheless, this value is still comparable to the spring constant reported for 2D graphene layers (1–5 N/m) [32]. Pure Aluminum has an elastic modulus of 70 GPa, which is more than an order of magnitude lower than graphene (~1 TPa). Since elastic modulus and spring constant are correlated by geometric parameters ($E = Kl/A$, where l and A length and cross-sectional area of the structure), the same order of magnitude difference is expected for spring constant of pure Al and graphene. However, due to the 3D architecture and intrinsic properties of graphene scaffold, the spring constant of Al/GrF heterostructure is remarkably enhanced compared to pure Al and matches the spring constant of 2D graphene sheets. This evidences that 3D graphene foam induces stiffening in the Al metal deposit, due to effective stress transfer during mechanical loading of the heterostructure. Therefore, the 3D graphene/metal framework developed in this study is an effective metamaterial which can be a useful filler material for imparting stiffness and flexibility to the lightweight structural materials.

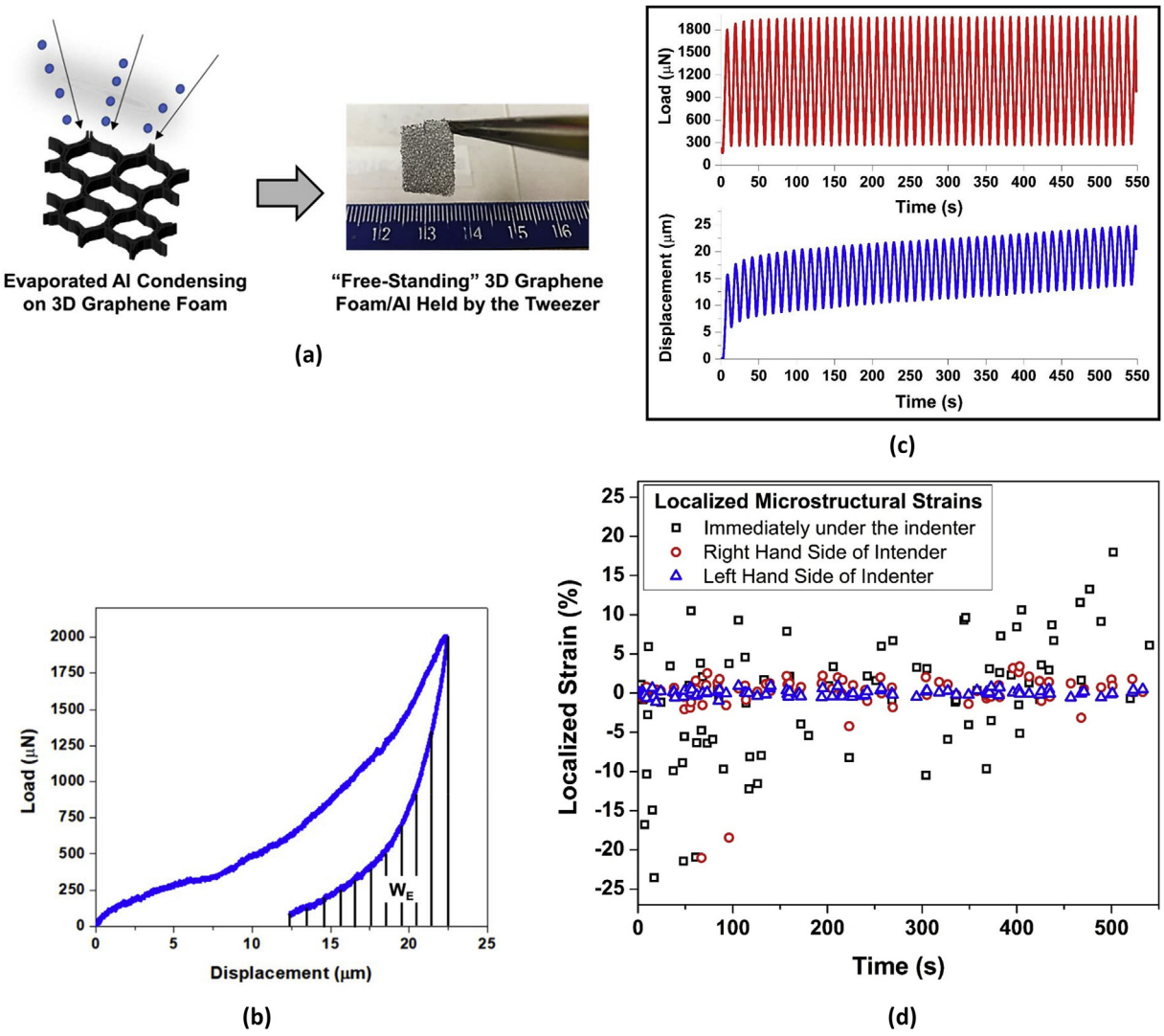

Fig. 3. (**a**) Schematic illustration of electron-beam evaporation process for developing stable, free-standing 3D Al/GrF metamaterial, (**b**) nanoindentation load-displacement curve for Al/GrF heterostructure, (**c**) cyclic loading/unloading profile and corresponding displacement response from Al/GrF for 50 indentation cycles, and (**d**) evolution of local strains under and around the indenter tip as a function of time obtained by DIC analysis of real-time SEM snapshots. (A colour version of this figure can be viewed online.)

Supplementary video related to this article can be found at https://doi.org/10.1016/j.carbon.2018.05.063.

The fatigue performance of Al/GrF was evaluated by indentation-induced cyclic loading-unloading. The material was subjected to ~1800 μN peak load and a total of 50 cycles (Fig. 3c). The real time SEM video of the test is provided as Supplementary Video V4. Similar to graphene foam, the Al/GrF heterostructure shows a highly elastic behavior, with an upward of 98% displacement recovered at the end of each cycle (Fig. 3c). The overall resistance to deformation was enhanced by Al backbone, as the net residual displacement at the end of 50 cycles was only ~20 μm, which is almost a third of residual deformation experienced by pristine foam (Fig. 2a). The material did not collapse, attesting excellent fatigue resistance of Al/GrF. DIC analysis of cyclic deformation revealed that the maximum deformation took place near the indenter tip (Fig. 3d). As the distance from the probe increased (>100 μm), the local strain was found to be very low, with $|\varepsilon_X| < 5\%$, compared to the immediate vicinity of the indenter where local strains could be as high as ±25% (plotted in Fig. 3d). This contrasts with the behavior observed for pristine graphene foam, which was found to exhibit marked deformation even at distances as high as 500 μm from the point of loading (Fig. 2c). The arrested long-distance deformation in Al/GrF is due to two reasons:

(i) The Al backbone restricts the deflection/compression of the otherwise very thin foam walls, resulting in enhanced resistance to deformation, and
(ii) Indentation loading can trigger small-scale local sliding between Al deposit and graphene foam wall at Al/GrF interface, which will lead to higher strains localized around the indenter but arrested long-distance stress transfer. The interfacial sliding also provides energy dissipation ability, which is desirable for damping and impact resistance in the mechanical structures.

Supplementary video related to this article can be found at https://doi.org/10.1016/j.carbon.2018.05.063.

3.3. Load-bearing ability of the metamaterial under tension

Indentation is a highly localized mechanical phenomenon. In order to assess the overall deformation behavior, Al/GrF was

subjected to *in-situ* tensile test and the deformation was monitored in real time under the SEM. The stress-strain plot for the tensile deformation is shown in Fig. 4a. The Al/GrF heterostructure was found to exhibit a tensile strength of ~75 kPa and a failure strain of ~9%. It is noteworthy that the strength of Al/GrF framework obtained here is more than 15 times the reported tensile strength for pristine graphene foam (4.8 kPa) [27]. This attests that Al acts as the structural backbone for 3D graphene framework by preventing

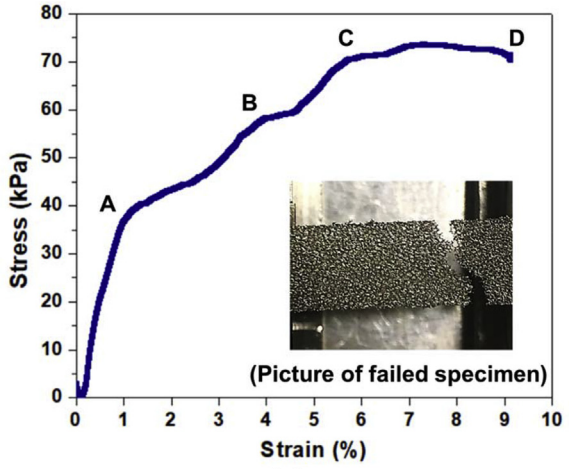

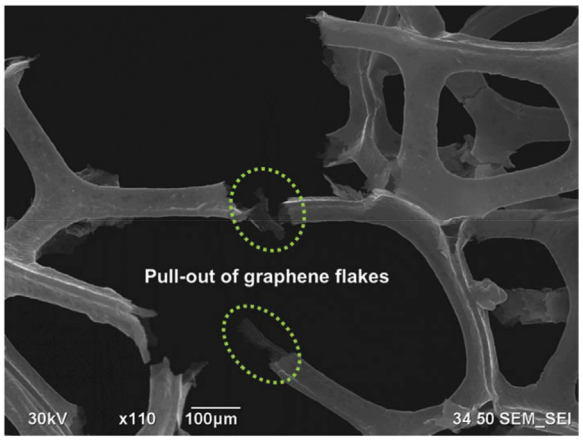

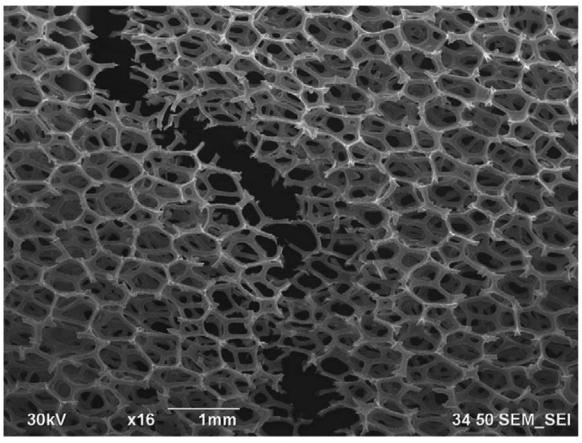

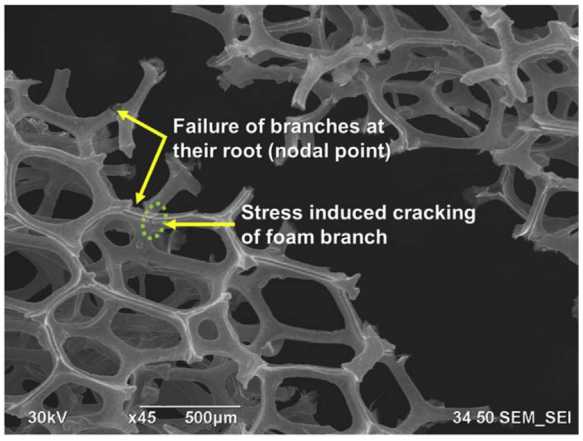

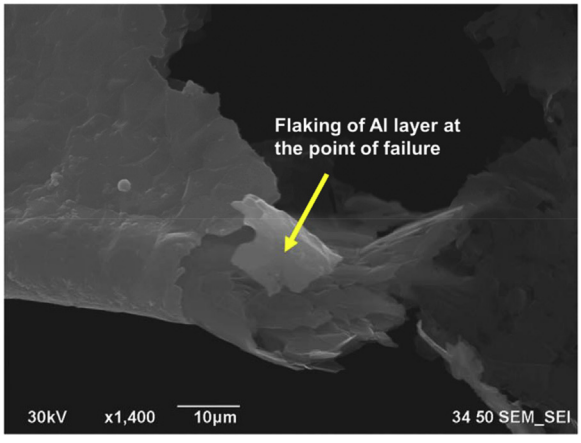

Fig. 4. **(a)** Tensile stress-strain plot for Al/GrF heterostructure (inset shows the optical picture of the failed specimen), **(b)** real-time SEM image during failure showing 45° fracture of 3D Al/GrF structure, **(c)** real-time SEM snapshot showing pull-out of graphene flakes at failure sites, **(d)** SEM micrograph showing tensile stress-induced cracking of foam branch and catastrophic failure at brittle nodal points, and **(e)** high magnification SEM micrograph near the failure site showing delamination and flaking of Al deposit. (A colour version of this figure can be viewed online.)

opening tearing of the foam at high stress concentration [35]. It is emphasized that the true cross-section area that bears the tensile stresses is extremely small (as the material is a porous foam). The intrinsic failure strength of the material is much higher than the apparent 'bulk' strength reported here.

The failure mechanisms in Al/GrF heterostructure were observed in real time under SEM. The fracture was found to occur at the plane ~45° to the tensile loading direction (Fig. 4b), suggesting shearing-type failure. Due to its ductile nature, Aluminum is known to deform by developing Lüders bands at ~45° to the direction of loading [36]. This failure plane typically experiences the maximum shear stress, $\tau_{max} = Y/2$, where Y is the tensile yield stress of the material. Aluminum has a lower yield strength (<11 MPa), compared to ultra-strong graphene (which has an intrinsic 2D crystal strength of 130 GPa [13]). Therefore, based on maximum shear stress theory, the determination of the failure plane is expected to be governed by Aluminum. However, the shearing will be complex due to interfacial stress transfer from Al to graphene. Stiff graphene foam walls will bear significant stresses during tensile loading, thereby augmenting the τ_{max} required to form slip bands in Al deposit. This is evidenced by the real-time SEM snapshot showing pull-out of graphene flakes during failure (Fig. 4c). Additionally, the graphene structure experiencing tensile stresses here is not monolayer graphene, but a 3D assembly. The failure is susceptible to the presence of defects/flaws in the structure, such as pre-existing cracks. Al deposit on graphene foam walls provides structural barrier to failure initiation at these defect sites. Nieto et al. demonstrated by *in-situ* tensile investigations that pre-existing cracks and points of discontinuity (in terms of graphene sheet arrangement) in the 3D foam branches severely compromise the load bearing ability [27]. Local failure mechanisms such as branch fracture, dramatic bending (almost 90° angle) and sheet sliding were observed at these defect sites. Deposition of Al layer (~1 μm thick) would restrict crack opening, fracture and delamination of flakes. This explains the enhanced tensile strength of Al/GrF compared to bare foam. Therefore, there are dual strengthening mechanisms at play: stiffening of Al due to graphene and healing of graphene foam flaws due to Al deposition. Intimate interfacial contact between the graphene foam walls and metal deposit is key to augment the mechanical properties of the 3D heterostructure.

During tensile stretching of the 3D assembly, the graphene foam branches experience twisting and bending, to align along the loading direction [27]. Nieto and co-workers reported that the branches align by rotating at the rate of ~0.59°/s. The stresses created during the rotation induces cracks in the branch, as shown in Fig. 4d. The nodes undergo more drastic rotation at rates exceeding 3°/s [27]. This abrupt alignment makes the brittle nodal points highly susceptible to failure, as shown in Fig. 4d. High magnification imaging of the failure points revealed that the crack initiation is followed by delamination and flaking of Al layer deposited on the foam (the outer flake marked in the SEM micrograph in Fig. 4e is Al, whereas the inner layers are graphene flakes). These delamination phenomena were rather limited, suggesting overall excellent bonding between the graphene foam walls and the deposited Al layer. These multi-scale deformation mechanisms in Al/GrF manifest as different regimes in the stress-strain plot (marked in Fig. 4a). The linear regime (up to point A) corresponds to the elastic stretching of 3D Al/GrF framework, with the elastic limit of ~35 kPa. This regime follows Hooke's law ($\sigma = E\varepsilon$) and the deformation is recoverable. Beyond point A, the deformation is plastic in nature. Due to its lower yield strength, the plastic deformation is initially expected to be dominated by the development of shear bands in Al. Therefore, region A to B corresponds to the yielding of Al. Thereafter, tensile stresses cause twisting and bending of graphene foam branches to align along the loading direction (regime B to C). Finally, there is stress-induced crack initiation and failure of nodes and branches, leading to the ultimate failure of the material (point D).

3.4. Modeling the mechanics of 3D graphene foam and associated metamaterials

To engineer 3D graphene-based metamaterials, ability to predict and model their mechanical properties as a function of geometry/architecture is very important. The scaling law for mechanical properties of open-cell foam structure provides an estimate of the strength of the material as a function of relative density: [9].

$$\frac{\sigma_T}{\sigma_{T_s}} = \left(\frac{\rho}{\rho_s}\right)^n \tag{6}$$

where σ_T and ρ are the tensile strength and mass density of foam structure, respectively, σ_{T_s} and ρ_s are the tensile strength and mass density of solid material, respectively, and n is the scaling exponent. Qin and co-workers determined the scaling exponent (n) for 3D graphene frameworks to be 2.01 ± 0.05 by molecular dynamic simulations [37]. Substituting this value of n to Eq. (6), the tensile strength of pristine graphene foam and Al/GrF heterostructure should be ~0.37 MPa and 5.77 MPa, respectively. However, the true experimental strength of graphene foam (0.0048 MPa) and Al/GrF (0.075 MPa) are 2 orders of magnitude lower than the computed strength. This discrepancy arises because the scaling law in Eq. (6) and the computational simulations for 3D graphene structures performed by Qin and co-workers only account for cellular architecture, but do not take into consideration the hollow structure of graphene foam branches and nodes (as seen in the inset of Fig. 1a). On comparing the theoretical and experimental strengths of pristine graphene foam and Al/GrF heterostructure, we notice that the theoretical strength (σ_{th}) is ~77 times the experimental strength (σ_{exp}). The mismatch in properties is because of the fact that the true cross section area that bears the load is much lower due to hollow branches of graphene foam (in addition to the open cells). To overcome this discrepancy between the theory and experiments, a geometric correction factor (f_G) needs to be introduced for estimating the strength of graphene foam and derived architectures. We propose a modified scaling law, with the correction factor f_G, for predicting the mechanical strength of cellular and hollow 3D graphene frameworks:

$$\frac{\sigma_T}{\sigma_{T_s}} = \frac{1}{f_G}\left(\frac{\rho}{\rho_s}\right)^{2.01\pm0.05} \tag{7}$$

Dividing the theoretical strength by the factor f_G will correct the overestimation of strength of the hollow-cellular foam. This factor accounts for the reduced, true cross-section area that is available to sustain the mechanical load. Based on the tensile investigations in this study, the value of f_G is found to be ~77 for the macroporous graphene foam structure (using Eq. (7) above). This empirically derived value of correction factor appears to hold true for both pristine foam [27] as well as Al/GrF heterostructure. However, it must be emphasized that any generalization regarding the value of this correction factor should be preceded by rigorous experimental and computational evaluation. Molecular dynamic simulations for 3D hollow and cellular foams can also be helpful for determining the values of this geometric factor. The modified scaling law proposed here will be a useful tool for engineering new metamaterials based on 3D graphene foam framework. This scaling law can predict the mechanics of graphene foam-based metallic, ceramic as well as polymeric heterostructures, as the proposed equation depends only on the geometry/architecture and relative densities of the materials.

4. Conclusion

We have developed highly elastic, flexible and fatigue-resistant 3D Graphene/Metal Metamaterial (GMM) based on macroporous graphene foam and lightweight Aluminum. *In-situ* mechanical investigations revealed that graphene foam exhibits at least 3 times higher spring constant compared to 2D graphene sheets, making the 3D Al/GrF metamaterial ultra-stiff. The interconnected network of nodes and branches facilitates long-distance stress-transfer and prevents localized failure. The structure is highly fatigue-resistant, with more than 98% of displacement recovery at the end of each loading/unloading cycle. *In-situ* tensile investigation revealed dual strengthening mechanisms, where stress transfer from Al layer to graphene scaffold enhances the load bearing ability and Al deposit on graphene foam provides a ductile backbone that prevents brittle failure. The mechanical properties of the proposed GMM can be tailored by varying the thickness of the metal deposit on 3D graphene scaffold. We proposed a modified scaling law for modeling mechanical strength of hollow, cellular foams. The 3D metamaterial developed in this study can be a game-changing candidate for developing flyweight metallic structures with unprecedented elasticity, stiffness and fatigue-resistance.

Acknowledgements

PN and AA acknowledge the Engineering Research Centers Program of the National Science Foundation under NSF Cooperative Agreement No. EEC-1647837. BB acknowledges the Office of Naval Research DURIP grant (N00014-16-1-2604) for establishing in-situ nanoindenter facility at FIU. PN thanks Florida International University (FIU) Graduate School for the Presidential Fellowship award. The authors also acknowledge Dr. Dawanne Poree, Program Manager of Polymer Chemistry at the US Army Research Office and W911NF-15-1-0458 grant. Advanced Materials Engineering Research Institute (AMERI) at FIU is acknowledged for the research facilities used in this study.

References

[1] T. Frenzel, M. Kadic, M. Wegener, Three-dimensional mechanical metamaterials with a twist, Science 358 (2017) 1072–1074.
[2] Z.G. Nicolaou, A.E. Motter, Mechanical metamaterials with negative compressibility transitions, Nat. Mater. 11 (2012) 608–613.
[3] J.L. Silverberg, A.A. Evans, L. McLeod, R.C. Hayward, T. Hull, C.D. Santangelo, et al., Using origami design principles to fold reprogrammable mechanical metamaterials, Science 345 (2014) 647–650.
[4] M. Eidini, G.H. Paulino, Unraveling metamaterial properties in zigzag-base folded sheets, Sci. Adv. 1 (2015), e1500224.
[5] A. Rafsanjani, A. Akbarzadeh, D. Pasini, Snapping mechanical metamaterials under tension, Adv. Mater. 27 (2015) 5931–5935.
[6] X. Zheng, H. Lee, T.H. Weisgraber, M. Shusteff, J. DeOtte, E.B. Duoss, et al., Ultralight, ultrastiff mechanical metamaterials, Science 344 (2014) 1373–1377.
[7] J.-H. Lee, J.P. Singer, E.L. Thomas, Micro-/Nanostructured mechanical metamaterials, Adv. Mater. 24 (2012) 4782–4810.
[8] X. Zheng, W. Smith, J. Jackson, B. Moran, H. Cui, D. Chen, et al., Multiscale metallic metamaterials, Nat. Mater. 15 (2016) 1100–1106.
[9] K. Davami, L. Zhao, E. Lu, J. Cortes, C. Lin, D.E. Lilley, et al., Ultralight shape-recovering plate mechanical metamaterials, Nat. Commun. 6 (2015) 10019.
[10] S.R. Bakshi, D. Lahiri, A. Agarwal, Carbon nanotube reinforced metal matrix composites-a review, Int. Mater. Rev. 55 (2010) 41–64.
[11] A. Nieto, A. Bisht, D. Lahiri, C. Zhang, A. Agarwal, Graphene reinforced metal and ceramic matrix composites: a review, Int. Mater. Rev. 62 (2017) 241–302.
[12] P. Nautiyal, C. Rudolf, A. Loganathan, C. Zhang, B. Boesl, A. Agarwal, Directionally aligned ultra-long boron nitride nanotube induced strengthening of aluminum-based sandwich composite, Adv. Eng. Mater. 18 (2016) 1747–1754.
[13] C. Lee, X. Wei, J.W. Kysar, J. Hone, Measurement of the elastic properties and intrinsic strength of monolayer graphene, Science 321 (2008) 385–388.
[14] Q. Zhang, D. Lin, B. Deng, X. Xu, Q. Nian, S. Jin, et al., Flyweight, superelastic, electrically conductive, and flame-retardant 3D multi-nanolayer graphene/ceramic metamaterial, Adv. Mater. 29 (2017), 1605506.
[15] K. Shehzad, Y. Xu, C. Gao, X. Duan, Three-dimensional macro-structures of two-dimensional nanomaterials, Chem. Soc. Rev. 45 (2016) 5541–5588.
[16] L. Qiu, J.Z. Liu, S.L.Y. Chang, Y. Wu, D. Li, Biomimetic superelastic graphene-based cellular monoliths, Nat. Commun. 3 (2012) 1241.
[17] L. Embrey, P. Nautiyal, A. Loganathan, A. Idowu, B. Boesl, A. Agarwal, Three-dimensional graphene foam induces multifunctionality in epoxy nanocomposites by simultaneous improvement in mechanical, thermal and electrical properties, ACS Appl. Mater. Interf. 9 (2017) 39717–39727.
[18] Y. He, W. Chen, X. Li, Z. Zhang, J. Fu, C. Zhao, et al., Freestanding three-dimensional graphene/MnO_2 composite networks as ultralight and flexible supercapacitor electrodes, ACS Nano 7 (2013) 174–182.
[19] Z. Chen, W. Ren, L. Gao, B. Liu, S. Pei, H.-M. Cheng, Three-dimensional flexible and conductive interconnected graphene networks grown by chemical vapor deposition. Nature Mater. 10, 424–428.
[20] Y. Zhang, Y. Huang, T. Zhang, H. Chang, P. Xiao, H. Chen et al., Broadband and tunable high-performance microwave absorption of an ultralight and highly compressible graphene foam. Adv. Mater. 27, 2049–2053.
[21] A. Nieto, R. Dua, C. Zhang, B. Boesl, S. Ramaswamy, A. Agarwal, Three dimensional graphene foam/polymer hybrid as a high strength biocompatible scaffold, Adv. Funct. Mater. 25 (2015) 3916–3924.
[22] P. Nautiyal, B. Boesl, A. Agarwal, Harnessing three dimensional anatomy of graphene foam to induce superior damping in hierarchical polyimide nanostructures, Small 13 (2017), 1603473.
[23] J. Bustillos, C. Zhang, B. Boesl, A. Agarwal, Three-dimensional graphene foam-polymer composite with superior deicing efficiency and strength, ACS Appl. Mater. Interf. 10 (2018) 5022–5029.
[24] H. Fang, Y. Zhao, Y. Zhang, Y. Ren, S.-L. Bai, Three-dimensional graphene foam-filled elastomer composites with high thermal and mechanical properties, ACS Appl. Mater. Interf. 9 (2017) 26447–26459.
[25] W. Park, X. Li, N. Mandal, X. Ruan, Y.P. Chen, Compressive mechanical response of graphene foams and their thermal resistance with copper interfaces, APL Materials 5 (2017), 036102.
[26] C. Wang, C. Zhang, S. Chen, The microscopic deformation mechanism of 3D graphene foam materials under uniaxial compression, Carbon 109 (2016) 666–672.
[27] A. Nieto, B. Boesl, A. Agarwal, Multi-scale intrinsic deformation mechanisms of 3D graphene foam, Carbon 85 (2015) 299–308.
[28] P. Nautiyal, B. Boesl, A. Agarwal, The mechanics of energy dissipation in a three-dimensional graphene foam with macroporous architecture, Carbon 132 (2018) 59–64.
[29] T.A. Schaedler, A.J. Jacobsen, A. Torrents, A.E. Sorensen, J. Lian, J.R. Greer, L. Valdevit, W.B. Carter, Ultralight metallic microlattices, Science 334 (2011) 962–965.
[30] M.G. Rashed, M. Ashraf, R.A.W. Mines, P.J. Hazell, Metallic microlattice materials: a current state of the art on manufacturing, mechanical properties and applications, Mater. Des. 95 (2016) 518–533.
[31] K.K. Jha, N. Suksawang, A. Agarwal, A new insight into the work-of-indentation approach used in the evaluation of material's hardness from nanoindentation measurement with Berkovich indenter, Comput. Mater. Sci. 85 (2014) 32–37.
[32] I.W. Frank, D.M. Tanenbaum, A.M. van der Zande, P.L. McEuen, Mechanical properties of suspended graphene sheets, J. Va. Sci. Technol. B 25 (2007) 2558–2561.
[33] D. Jang, L.R. Meza, F. Greer, J.R. Greer, Fabrication and deformation of three-dimensional hollow ceramic nanostructures, Nat. Mater. 12 (2013) 893–898.
[34] V.K. Khanna, Adhesion-delamination phenomena at the surfaces and interfaces in microelectronics and MEMS structures and packaged devices, J. Phys. D Appl. Phys. 44 (034004) (2011).
[35] D. Pan, C. Wang, T.-C. Wang, Y. Yao, Graphene foam: uniaxial tension behavior and fracture mode based on a mesoscopic model, ACS Nano 11 (2017) 8988–8997.
[36] P. Kelly, Solid State Mechanics Lecture Notes, The University of Auckland, Auckland, 2013.
[37] Z. Qin, G.S. Jung, M.J. Kang, M.J. Buehler, The mechanics and design of a lightweight three-dimensional graphene assembly, Sci. Adv. 3 (2017), e1601536.